# Fabrication and Optimization of 3D Printed Gelatin Methacryloyl Microneedle Arrays Based on Vat Photopolymerization

Dilruba Baykara[a,b,1], Tuba Bedir[a,c,1], Elif Ilhan[a,d], Mehmet Eren Mutlu[a,e], Oguzhan Gunduz[a,c], Roger Narayan[f*], Cem Bulent Ustundag[b*]

[a]Center for Nanotechnology and Biomaterials Application and Research (NBUAM), Marmara University, 34722, Istanbul, Turkey

[b]Department of Bioengineering, Faculty of Chemical and Metallurgical Engineering, Yildiz Technical University, 34210, Istanbul, Turkey

[c]Department of Metallurgical and Materials Engineering, Faculty of Technology, Marmara University, 34722, Istanbul, Turkey

[d]Department of Bioengineering, Faculty of Engineering, Marmara University, 34722, Istanbul, Turkey

[e]Department of Metallurgical and Materials Engineering, Faculty of Chemical and Metallurgical Engineering, Yildiz Technical University, 34210, Istanbul, Turkey

[f]Joint Department of Biomedical Engineering, University of North Carolina, 27599, Chapel Hill, USA

[*]Corresponding authors: cbustundag@gmail.com, rjnaraya@ad.unc.edu

# Abstract

Microneedles (MNs) are micrometer-sized arrays that can penetrate the skin in a minimally invasive manner; these devices offer tremendous potential for the transdermal delivery of therapeutic molecules. Although there are many conventional techniques for manufacturing MNs, most of them are complicated and can only fabricate MNs with specific geometries, which restricts the ability to adjust the performance of the MNs. Herein, we present the fabrication of gelatin methacryloyl (GelMA) MN arrays using the vat photopolymerization 3D printing technique. This technique allows for the fabrication of high-resolution and smooth surface MNs with desired geometries. The existence of methacryloyl groups bonded to the GelMA was verified by $^{1}$H NMR and FTIR analysis. To examine the effects of varying needle heights (1000 μm, 750 μm, and 500 μm) and exposure times (30 s, 50 s, and 70 s) on GelMA MNs, the height, tip radius, and angle of the needles were measured; their morphological and mechanical properties were also characterized. It was observed that as the exposure time increased, the height of the MNs increased; moreover, sharper tips were obtained and tip angles decreased. In addition, GelMA MNs exhibited good mechanical performance with no breakage up to 0.3 mm displacement. These results indicate that 3D printed GelMA MNs have great potential for transdermal delivery of various therapeutics.



**Keywords:** Gelatin methacryloyl; Hydrogel; Microneedle; Vat photopolymerization 3D printing

# Introduction

Microneedles (MNs) are skin-penetrating painless transdermal drug delivery systems, which consist of sub-millimeter-sized needles [1,2]. These devices are considered a minimally invasive medical intervention due to their microscale size [3,4]. MN arrays can be designed with different sizes and shapes; these devices can play an essential role in the delivery of several therapeutic molecules such as small molecules, biomacromolecules, and nanoparticles for treating various diseases [5,6]. This next generation drug delivery system has attracted attention in recent years due to its advantages such as ease of administration, low cost, excellent therapeutic efficacy, and relative safety [7,8].

Conventional MN fabrication techniques include molding-based techniques [9], photolithography [10], micro-milling [11], and drawing lithography [12]. However, most of these fabrication techniques can only produce MNs with specific geometries, which limits the capacity to change MN properties such as shape, height, and needle spacing [13,14]. Furthermore, these techniques are complicated and often require long production processes, manual processing steps, costly equipment, and intensive labor efforts [15,16]. Additive manufacturing is a fabrication technique that overcomes many of the design and production limitations associated with conventional MN processing methods [16]. 3D printing (more formally referred to as additive manufacturing) approach in which MNs designed in a computer-aided program are produced in a layer by layer manner. 3D printing is also associated with advantages such as high resolution and good cost efficiency [17]. Digital light processing (DLP) 3D printing technology, which is based on vat photopolymerization, enables the formation of a structure by curing layers of an ultraviolet (UV) sensitive polymer [18]. The projector (digital light micromirror) in the device converts an image signal of the cross-section of the object into a digital signal; the photocuring process takes place using this digital signal [19]. Using a projector allows for faster print times since it involves curing each full layer of

material in one step [20]. This technique allows only photo-curable materials to be utilized as feedstock materials [21]. Moreover, MN production with high resolution on a micrometer scale along with processing of surfaces with smooth features can be performed with this technique [22]. For example, Shin et al. have demonstrated the fabrication of protein-based MNs using the DLP-based 3D printing technique [23]. In addition, Erkus et al. prepared GelMA MNs loaded with amoxicillin using DLP 3D printing [24].

The first-generation materials used in MN fabrication include silicon, metals, ceramics, and glasses [25]. These materials have drawbacks in MN manufacturing such as limited drug loading capabilities and expensive production methods [26]. When compared to other materials, polymeric forms of MNs (soluble and hydrogel-forming MNs) are remarkable due to their unusual properties such as biodegradability, biocompatibility, and an absence of toxicity [27,28]. Polymeric hydrogels used as drug delivery systems are defined as three-dimensional network formulations of natural and synthetic polymers [29]. The network-like porous structure of these structures enhances the loading and controlled release of drugs under proper conditions. It is advantageous to be able to control the drug release profile and performance of hydrogel MNs, which have different degradation profiles and swelling properties [30]. Gelatin methacryloyl (GelMA), obtained by modifying natural gelatin, is a hydrogel that can be crosslinked using UV light or visible light with exposure to a photoinitiator [31]. It is an ideal material for the production of MNs due to its biocompatibility, tunable mechanical properties, printability, low cost, and desirable drug delivery properties [32]. In addition, GelMA hydrogel has powerful biological properties such as supporting functional cell growth [33]. During the GelMA synthesis, many amino groups in the side chains of gelatin are replaced with methacryloyl groups in the structure of methacrylate anhydride (MAA). After synthesis, the methacryloyl groups of gelatin impart crosslinking properties [34]. The interaction of GelMA

with UV light in the presence of a photoinitiator results in the formation of a hydrogel with excellent thermostability [35].

When using photopolymers in 3D printing systems, the use of a photoinitiator is necessary to facilitate the crosslinking process [36]. During photocrosslinking of photopolymers, the photoinitiator absorbs UV light to generate free radicals; these free radicals polymerize the photosensitive resin to form the polymer network [37]. Photoinitiators such as Irgacure 2959, LAP, VA086, and Eosin-Y are commonly used owing to their cytocompatibility with living cells [25]. In particular, LAP is a remarkable photoinitiator for biomedical applications due to its water solubility, low toxicity, and absorbance of both 365 and 405 nm light [38].

Herein, GelMA MN arrays with the desired design at different exposure times were developed using the DLP-based 3D printing technique. As far as is known, no previous studies have been reported in the literature regarding DLP-based GelMA MN arrays fabricated at different heights and exposure times. In the current study, after the GelMA was synthesized, the design, printing conditions, and post-printing processes of MNs were optimized. Mechanically and morphologically optimized GelMA MNs may represent an attractive component in new types of transdermal drug delivery systems. The findings of this study can offer insight into design applications aimed at optimizing 3D-printed MNs for adjustable and customizable drug delivery.

# Materials and methods

## Materials

Gelatin Type A obtained from porcine skin, methacrylic anhydride (MAA), lithium phenyl-2,4,6-trimethyl-benzoyl phosphinate (LAP), and dialysis membrane (with a cut-off value of 14 kDa and an average flat width of 43 mm) were purchased from Sigma–Aldrich (Darmstadt, Germany). Sodium carbonate, sodium hydroxide, and hydrochloric acid fuming 37% were

obtained from Merck KGaA (Darmstadt, Germany). Sodium hydrogen carbonate (>99.7%) was obtained from ISOLAB (Eschau, Germany). Phosphate-buffered saline (PBS, pH 7.4) was purchased from ChemBio (Turkey).

## Synthesis of Gelatin Methacryloyl (GelMA)

10% (w/v) solution of type A gelatin was prepared in 0.1 M carbonate bicarbonate buffer (0.1 M CB buffer containing 3.18 g sodium carbonate and 5.86 g sodium bicarbonate in 1 L of distilled water, pH 9) at 60 °C. Then, 0.1 mL of methacrylic anhydride (MAA) per gram of gelatin was added to the gelatin solution and allowed to react for 3 h at 50 °C under constant stirring. The reaction was then terminated by adjusting the pH to 7.4 (Fig 1). The obtained solution was dialyzed with a 14 kDa molecular-weight-cutoff (MWCO) membrane against distilled water for 2 days at 40 °C. Dialysis of GelMA solution helped to remove unreacted MAA and methacrylic acid byproducts. After the dialysis step, the solution was lyophilized for three days and stored at +4 °C until use.

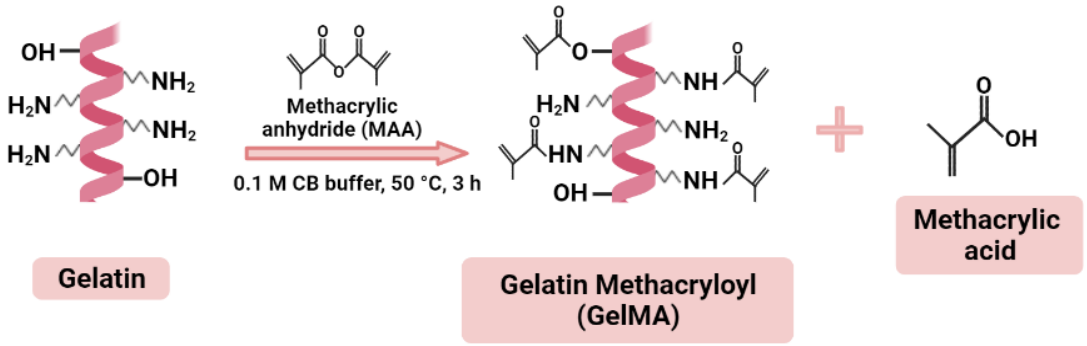


**Fig 1.** Synthesis route of GelMA.

## Determination of GelMA degree of substitution

The degree of substitution (DS) of GelMA was investigated using $^{1}H$ NMR spectroscopy (Bruker Avance III 600 MHz, Bremen, Germany). Both gelatin and GelMA were dissolved at a 10 mg/mL concentration in $D_2O$; $^{1}H$ NMR spectra were obtained at a frequency of 600 MHz

and at room temperature. The DS of GelMA was calculated according to the following equation:

$$DS(\%) = \left(1 - \frac{peak\ area\ of\ GelMA\ lysine\ methylene}{peak\ area\ of\ gelatin\ lysine\ methylene}\right) x100 \quad \text{Eq(1)}$$

# Fourier Transform Infrared Spectroscopy (FTIR)

The chemical structure of gelatin and GelMA were investigated using Fourier transform infrared spectroscopy (FTIR, FT/IR-ATR 4700, Jasco, Easton, MD, USA) at room temperature. Spectra were obtained between 450 and 4000 $cm^{-1}$ range at a resolution of 4 $cm^{-1}$.

# Rheological characterization of GelMA

The rheological behavior of GelMA hydrogel was analyzed using a digital rheometer (Discovery HR2, TA Instruments, New Castle, DE, USA). The oscillation mode was selected to determine the temperature dependence of the shear modulus of the GelMA hydrogel. The temperature ramp test was performed over a range of 37-15 °C (heating rate 1 °C/min) with a frequency of 1 Hz and strain of 1%. The frequency sweep test was carried out at an angular frequency of 0.01–100 rad/s with a constant frequency (1 Hz) and strain (1%). The viscosity of GelMA hydrogel was measured by varying the shear rate from 1 to 100 1/s.

# Design and fabrication of GelMA MNs

Computer-aided design (CAD) files of conical MN arrays with three different needle heights of 1000 μm, 750 μm, and 500 μm were prepared using SolidWorks 2020 (Dassault Systèmes SE, Vélizy-Villacoublay, France). MNs were designed to be 600 μm wide at the base and were attached to a solid 10×10×1 mm substrate consisting of a 6×6 array. The MN designs were converted to the .stl file format and sliced using Chitubox (Shenzhen Chuangbide Technology Co., Ltd., Shenzhen City, China), the software for the 3D printer (Fig 2a). A commercially

accessible DLP-based 3D printer (Phrozen Shuffle 4K, Phrozen Tech Co Ltd., Hsinchu, Taiwan) was utilized to manufacture the MNs. A 12 mW/cm$^2$ light intensity and 405 nm light wavelength were used for printing the MNs. Subsequently, MNs with varying heights were subjected to exposure times of 30 s, 50 s, and 70 s, respectively.

For the printing of MNs, a 10% (w/v) GelMA solution was prepared with PBS solution under constant stirring at 40 °C for 30 min. The photoinitiator (LAP) at a 0.5 % concentration was added to the GelMA solution and mixed for 10 min. Next, the mixture was brought to room temperature (~25 °C) and transferred to the tank of the DLP printer (Figure 2b). MNs were printed according to the parameters given above. The fabricated 3D-printed MNs were dried in the dark at room temperature for 24 h and kept in a dehumidified container until the characterization activities (Fig 2c).

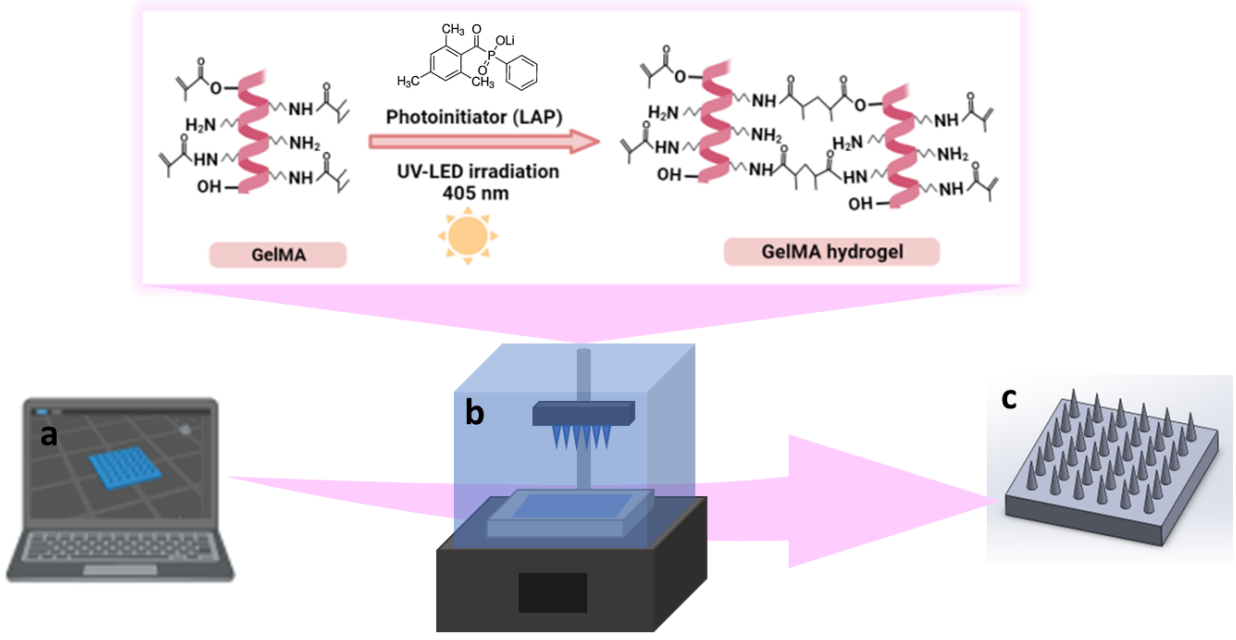


**Fig 2. Schematic representation of the design and fabrication of GelMA MNs, (a) designing of CAD model, (b) photocrosslinking of GelMA hydrogel during DLP printing, (c) 3D printed GelMA MNs.**

## Morphological characterization of GelMA MNs

The height, tip radius, angle, and surface characterization of each MN were evaluated using a scanning electron microscope (SEM) (EVA MA 10, Zeiss, Jena, Germany). Prior to analysis, the surfaces of the MNs were coated with gold using a spray coating machine (SC7620, Quorum, Laughton, East Sussex, UK) for 120 seconds.

## Mechanical analysis for GelMA hydrogels and GelMA MNs

10% GelMA hydrogels prepared with different exposure times (30 s, 50 s, and 70 s) were characterized in terms of their compression stiffness using a compression testing machine (EZ-LX, Shimadzu, Kyoto, Japan). Cylindrical specimens of GelMA (8 mm in diameter and 6 mm in height) were tested; a rate of 1 mm/min and a maximum strain of 60% were used in these studies. Compressive modulus values were calculated from the initial linear region (0–20% of strain) of the obtained stress-strain curves. Each measurement was performed in triplicate and results are reported as mean ± standard deviation values.

The mechanical strength of GelMA MNs was analyzed with a compression testing machine (EZ-LX, Shimadzu, Kyoto, Japan ). MNs were placed on a stainless steel plate at a distance of 2 mm; an axial force was applied at a constant rate of 0.1 mm/min perpendicular to the axis of the MNs. The mechanical characteristics of MNs with different needle heights (1000 μm, 750 μm, and 500 μm) and different exposure times (30 s, 50 s, and 70 s) were profiled. All tests were performed in triplicate.

## Statistical analysis

The experiments were carried out at least in triplicate, and data are expressed as mean ± standard deviation (SD). Post-hoc one-way ANOVA with a Tukey-Kramer pair-wise comparison were employed for statistical analysis. A value of $p \leq 0.05$ is considered statistically significant, and additional significance is indicated by ** for $p < 0.01$ and *** for $p < 0.001$.

# Results and discussion

## Determination of GelMA degree of substitution

$^{1}$H NMR analysis was performed to verify the successful substitution of gelatin with methacryloyl groups (Fig 3a). Compared with the $^{1}$H NMR spectra of gelatin, the GelMA displayed new signals corresponding to the methacryloyl groups, labelled as orange (a+b), green (c) and purple (d). The signals at around chemical shifts of 5.3 and 5.6 ppm (a+b) were attributed to the acrylic protons (2H) of methacryloyl group grafted to lysine and hydroxylysine residues of the gelatin backbone. This result indicates the existence of C=C bonding in the anhydride structure, which is related to presence of the vinyl groups of methacrylate anhydride [39]. The signal at approximately 1.8 ppm (d) in the GelMA spectrum was assigned to the methyl protons (3H) of the grafted methacryloyl group. In addition, a decrease in the intensity of the signal at around 2.9 ppm (c), which was associated with the lysine methylene (2H) was observed in GelMA compared to gelatin [40,41]. As lysine is the reaction site, this finding was used to quantify the DS, which was estimated to be 75.4%.

## Fourier Transform Infrared Spectroscopy (FTIR)

The substitution of methacrylate groups to the gelatin chain in the structure of GelMA was further confirmed by FTIR analysis. The FTIR spectra of pure gelatin and GelMA are presented in Fig 3b. The FTIR spectrum of GelMA exhibits a sharp peak at 1630 $cm^{-1}$, corresponding to C=O stretching groups of amide I bond (labelled as yellow) [39]. The peak at 1546 $cm^{-1}$ is attributed to the N–H bending groups of the amide II bond (labelled as green); the peak at 1244 $cm^{-1}$ is related to the C–N stretching and N-H bending of the amide III bond (labelled as pink) [39,42]. Furthermore, the peak located in the range of 3200–3400 $cm^{-1}$ (labelled as blue) detected in GelMA is associated with the existence of peptide bonds (N–H stretching) and -OH

functional groups [43]. The shifts and changes identified in the GelMA peaks compared to pure gelatin indicated that the lysine groups of gelatin were successfully substituted by the methacrylate groups [44].

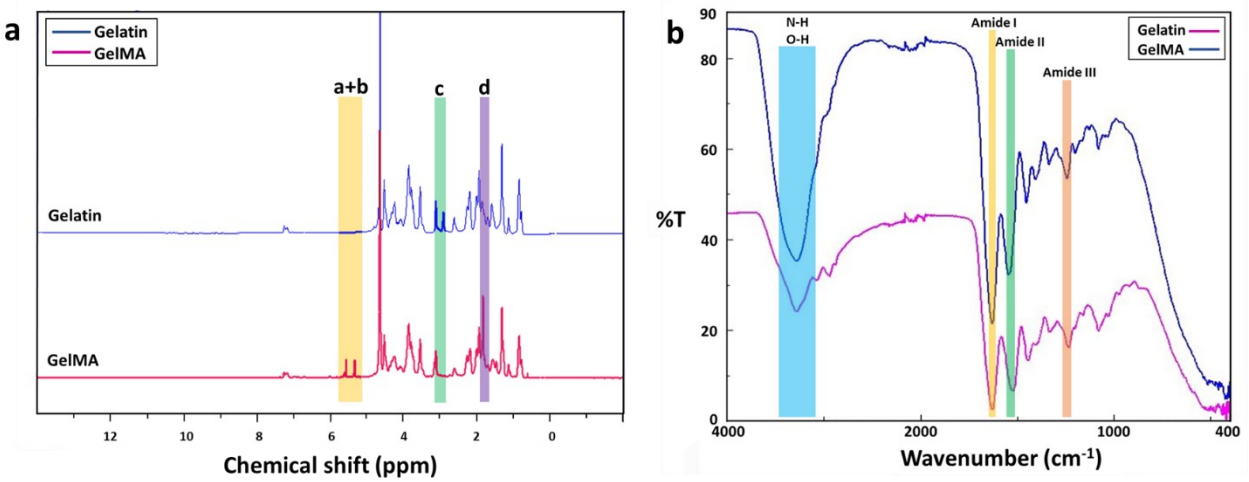


**Fig 3. $^{1}$H NMR spectra of gelatin and GelMA (a), FTIR spectra of gelatin and GelMA (b).**

## Rheological characterization of GelMA

To determine the viscoelastic properties of 10% (w/v) GelMA hydrogel, its shear moduli and viscosity were evaluated by rheological testing (Fig 4). The hydrogel demonstrated temperature-dependent gelation behavior (Fig 4a). The crossing of the storage modulus (G') and loss modulus (G") curves is the gelation temperature of the hydrogel. Below about 22 °C, the GelMA hydrogel exhibited solid characteristics (G' > G"). When the temperature was increased, the sol-gel transition occurred in the range of 22 °C (G' = G"); at higher temperatures, the hydrogel displayed liquid-like behavior (G" > G'). According to the results of the oscillation frequency sweep of the GelMA hydrogel tested in the angular frequency range of 0.01 rad/s to 100 rad/s, an increase was observed in both G' and G" with increasing frequency (Fig 4b). In Fig 4c, the viscosity decreased with increasing shear rate, supporting the shear-thinning behavior of the GelMA hydrogel [45].

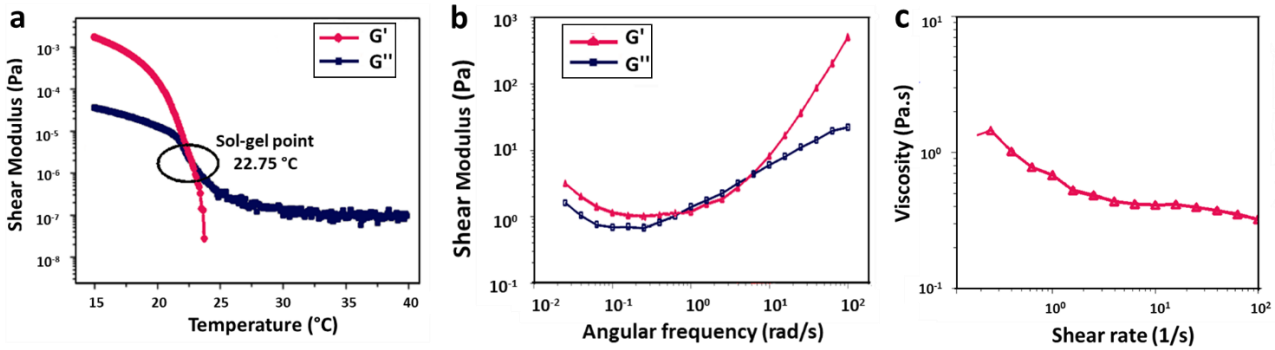


**Fig 4. Rheological analysis of 10% (w/v) GelMA hydrogel, (a) temperature ramp test, (b) frequency sweep test, and (c) rotational shear rate-viscosity measurement.**

## Morphological characterization of GelMA MNs

GelMA MNs designed with three different needle heights (h:1000 µm, 750 µm, and 500 µm) were fabricated with a DLP printer by utilizing three different exposure times (30 s, 50 s, and 70 s); SEM images of the obtained hydrogel MNs are shown in Fig 5. The effect of varying needle sizes and exposure times on GelMA MNs was investigated. As can be seen in Fig 5A, MNs with an exposure time of 30 s could not be fully printed as the light intensity may drop below the threshold as the sliced images approached the tip [46], preventing the processing of the conical structure. Incomplete MNs resulting from a short exposure time are not hard enough to penetrate the skin [47]. On the other hand, MNs exposed for 50 s were well-printed conical structures that exhibited a uniform and regular morphology. When the exposure time was increased to 70 s, the distance between the MNs decreased due to overexposure. In addition, the hardness of the MNs may increase as a result of the long exposure time [48].

In order to better observe the influences of changing needle sizes and exposure times on the printability of MNs, three parameters (e.g., height, tip radius, and angle) of the printed MNs were measured and presented in Fig 5B. The printability of MNs at different heights is important for adjusting the depth of penetration in the skin and changing the volume available

for the delivery of therapeutics [49]. It is seen that the experimental heights of MNs, which are designed with theoretical needle heights of 1000 μm (A), 750 μm (B), and 500 μm (C), respectively, are less than those of the corresponding designs (Fig 5B(a)). This finding may be due to the minimum UV dose necessary for photopolymerization as well as the manner in which a layer is produced [50]. The light that projects off each micromirror usually spreads to nearby pixels. Thus, the amount of light per unit area for large pieces (where light from surrounding pixels converge) is greater than those for small pieces. Therefore, the curing of small pieces is often not achieved [16]. Accordingly, since a vertically aligned needle exhibits a continuously decreasing cross-sectional slice in the x-y plane, the print may result in round-shaped tips before the full theoretical needle height is reached [50]. Similar results were noted by Johnson et al. in a study that involved the CLIP (Continuous Liquid Interface Production) printing system [51]. In addition, the heights of the MNs increased as the exposure time increased (from 30 s to 70 s) for all three needle sizes as confirmed by SEM images: (A) MNs increased from about 368.4 ± 5.6 μm to 586.9 ± 17.9 μm, (B) MNs increased from 312.2 ± 10.8 μm to 488.1 ± 2.9 μm, and (C) MNs increased from 197.8 ± 23.5 μm to 321.1 ± 7.4 μm.

Another important parameter that is necessary to ensure penetration of the MNs into the skin is the tip radius. The tip radius determines the sharpness of the MN [16]. Fig 5B(b) demonstrates that the tip radii of the printed MNs were in the range from ~30 μm to 36 μm. There appeared to be a tendency to decrease in tip radius with decreasing needle height (from 1000 μm to 500 μm) at the same exposure time. When measurement precision and error are taken into consideration, the difference is not substantial. Needle tips are particularly subject to needle-to-needle variability as a result of a lack of precision in printing [50]. Moreover, as expected, sharper tips were obtained as the exposure time increased for all three needle sizes. (C) MNs exhibited the sharpest needle tip with a tip radius of 30.6 ± 0.7 μm at 70 s. Since tip radii of 20-

40 μm are known to be of sufficient sharpness for skin penetration [52], the obtained tip radii can be said to be among the sharpest hydrogel needles printed using a DLP printing system.

The θ angle was the last design parameter measured. Regardless of the tip radius, this value measures the angle between needle sides. According to Fig 5B(c), the needle angle increased as needle height decreased for the same exposure time. As exposure time increased, the needle angle decreased for (A) MNs from 53.2 ± 3.7 to 48.2 ± 0.4, (B) MNs from 68.7 ± 3.5 to 52.2 ± 0.6, and (C) MNs 89.1 ± 1.2 to 67.3 ± 2.6, respectively. These results support the successful fabrication of GelMA MNs with different needle heights and exposure times using a DLP printer.

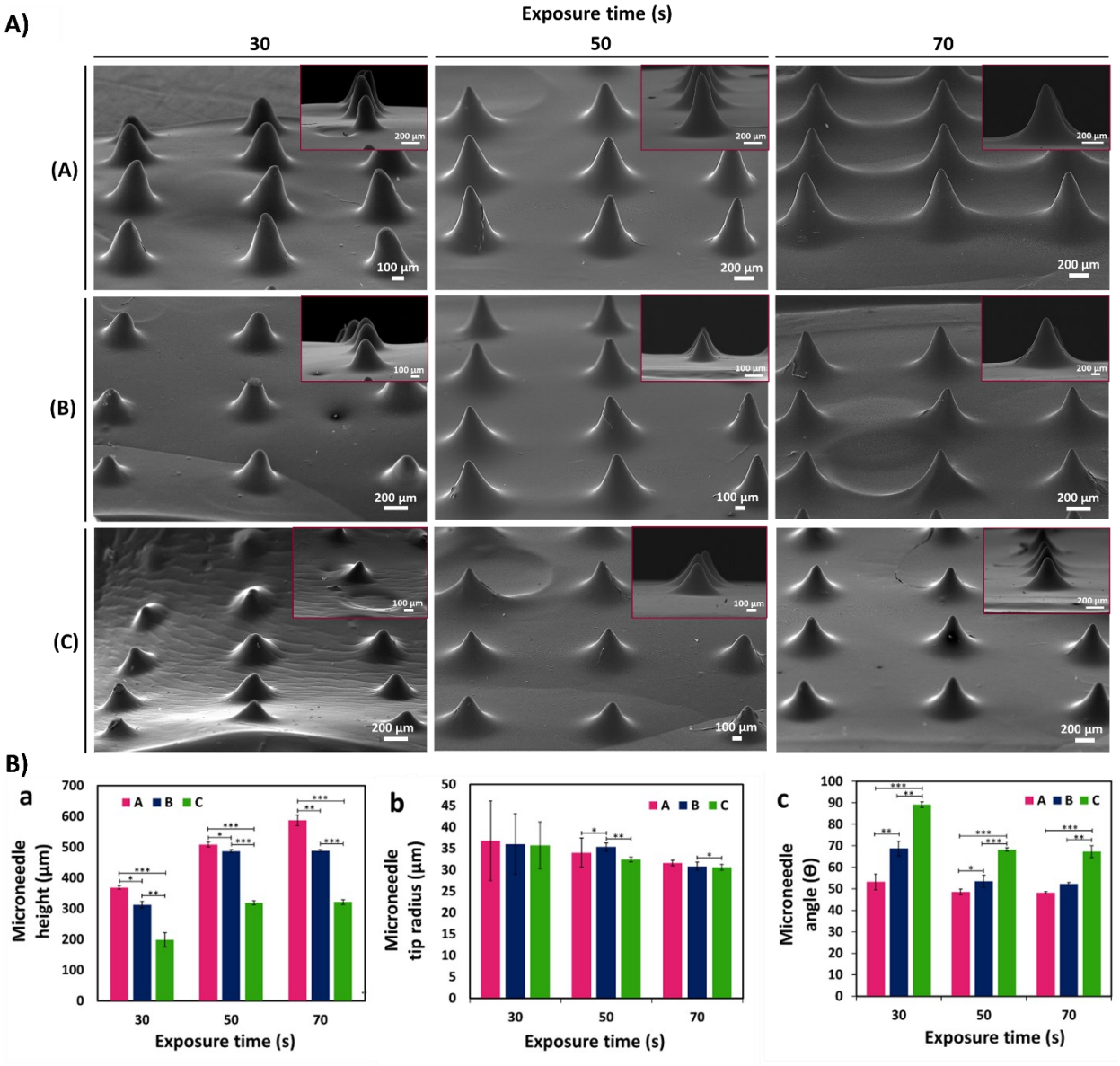


**Fig 5. A) SEM images of GelMA MNs designed in three different needle heights according to varying exposure times: (A) 1000 µm height, (B) 750 µm height, and (C) 500 µm height. B) Variation of (a) height (b) tip radius and (c) angle of GelMA MNs according to exposure times.** Statistical difference is indicated with $*p \leq 0.05$, $**p < 0.01$, and $***p < 0.001$. Error bars represent the standard deviations (SDs) of measurements performed on at least three samples.

## Mechanical analysis for GelMA hydrogels and GelMA MNs

Fig 6 shows the compressive stress-strain curves of GelMA hydrogels at different UV exposure times (30 s, 50 s, and 70 s). From the stress-strain curves, it was observed that the compressive strength increased by increasing the exposure time from 30 s to 70 s. As can be seen in Table 1, the GelMA hydrogel exposed to 70 s exhibits a higher modulus of compression than those exposed to 30 s and 50 s. Since polymerization is a kinetic process, longer exposure times enable greater completion of the polymerization reaction. Thus, longer polymerization times up to a certain threshold lead to a greater number of functional crosslinks, resulting in higher modulus of elasticity values [53]. Similar results for the GelMA hydrogel have been reported by Chansoria et al. [54]

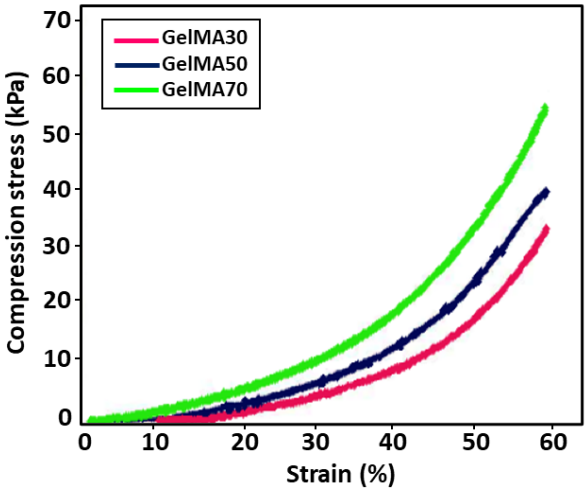


**Fig 6. Stress-strain curves for GelMA hydrogels at different UV exposure times (30 s, 50 s, and 70 s).**

**Table 1. Compressive modulus of elasticity from stress-strain curves for GelMA hydrogels at different UV exposure times.**

| Sample | Compressive modulus (kPa) | | |
|---|---|---|---|
| | **30 s** | **50 s** | **70s** |
| 10% (w/v) GelMA | 1.97 ± 0.12 | 3.72 ± 0.10 | 6.51 ± 0.10 |

The mechanical properties of MNs are critical for successful skin penetration [55]. The mechanical properties of GelMA MNs was investigated using a compression test. As shown in Fig 7, no discontinuity or breakage was observed in the displacement curves of the GelMA MNs up to the displacement value of 0.3 mm. In addition, there was no broken MN up to the value above. Makvandi et al. noted that transdermal MN patches should puncture the human stratum corneum (~10 to 20 μm) without tearing or bending during penetration [56]. This result implies that the produced MNs exhibit appropriate toughness for skin penetration [24]. Moreover, an increase in mechanical strength with an increase of exposure time (from 30 s to 70 s) for the same needle size groups was one of the findings supported by previous studies [46, 57]. The amount of force required to induce the same level of compression in materials with increased crosslinking density was higher, indicating that increasing the crosslinking time improved the mechanical strength of MNs significantly. Therefore, the quantity of crosslinking in the GelMA MNs is a key factor in determining the mechanical qualities of MNs [48]. By profiling the applied compressive force and the displacement of the MNs, Zhou et al. found that longer crosslinking times resulted in higher crosslinked network densities, which required greater force to achieve similar displacement values [58]. In another study, when the difference in the mechanical properties of the produced GelMA MNs was examined without any UV crosslinking and after 15 s of crosslinking, it was demonstrated that the mechanical strength of the 15 s light-cured GelMA MNs increased significantly [59].

Moreover, Fig 7 demonstrates the displacement of MNs at different heights exposed to UV against an applied force. It was determined that the longest MNs in each group, among the MNs produced in three different sizes, tended to move the most. It can be observed that the displacement values of (A) MNs were high among their groups in those exposed to 30 s of UV, (A) in those exposed to 50 s of UV, and (A) in those exposed to 70 s. It should be noted the MNs produced by Xenikakis et al. with a maximum length of 930 μm at applied forces over 60

N were severely bent and deteriorated compared to short needles [60]. In a different study, MNs produced with the same base diameter of 750 µm and 500 µm had their displacements measured as 0.0255 and 0.127 mm, respectively, when 0.1 N force was applied. This result proves that higher MNs exhibited more displacement under the same force [61].

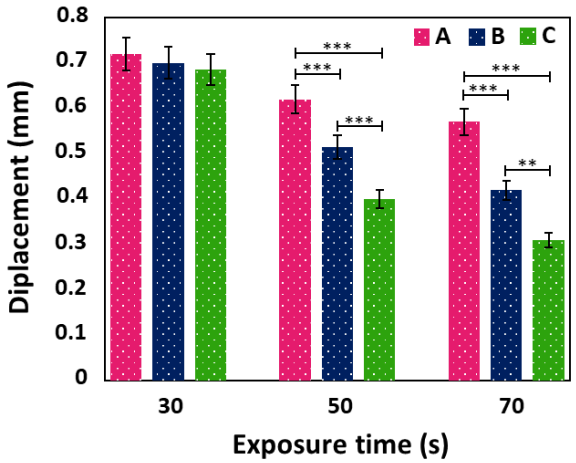


**Fig 7. Displacement curve of GelMA MNs with different needle heights according to varying exposure times.** Statistical difference is indicated with $*p \leq 0.05$, $**p < 0.01$, and $***p < 0.001$. Error bars represent the standard deviations (SDs) of measurements performed on at least three samples.

# Conclusions

In this study, GelMA MNs were successfully fabricated with desired geometries at high resolution using the DLP-based 3D printing technique. Smooth surface MNs with different heights (1000 µm, 750 µm and 500 µm) and different UV exposure times (30 s, 50 s, and 70 s) were obtained. $^{1}$H NMR analysis proved the existence of methacryloyl groups attached to GelMA; these results were also supported by FTIR analysis. According to the morphological analysis, it was observed that MNs had higher needle heights and sharper tips as the exposure time increased; the tip angles decreased accordingly. Furthermore, the compression test results showed that increasing the exposure time decreased the amount of displacement. Therefore, it

370 can be said that GelMA MNs at lower heights showed less displacement when equal force was
371 applied. In addition, GelMA MNs demonstrated good mechanical performance without any
372 breakage up to 0.3 mm displacement. These findings indicate that the 3D-printed GelMA MNs
373 have the potential for use in a variety of transdermal drug delivery systems.


374 # Acknowledgements

375 The authors wish to thank the Biomedical Imaging and Diagnostic Systems Development
376 Laboratory at Marmara University, Istanbul.


377 # Competing Interests

378 The authors have declared that no competing interests exist.


379 # Financial Disclosure

380 The funders had no role in study design, data collection and analysis, decision to publish, or
381 preparation of the manuscript.


382 # Data Availability

383 The datasets generated during and/or analyzed during the current study are available from the
384 corresponding author on reasonable request.

385 # References


386 1. Kim Y-C, Park J-H, Prausnitz MR. Microneedles for drug and vaccine delivery. Adv
387 Drug Deliv Rev. 2012;64: 1547–1568. doi:10.1016/j.addr.2012.04.005

388 2. Mutlu ME, Ulag S, Sengor M, Daglılar S, Narayan R, Gunduz O. Electrosprayed
389 Collagen/Gentamicin nanoparticles coated microneedle patches for skin treatment.

Mater Lett. 2021;305: 130844. doi:https://doi.org/10.1016/j.matlet.2021.130844

3. Krieger KJ, Bertollo N, Dangol M, Sheridan JT, Lowery MM, O'Cearbhaill ED. Simple and customizable method for fabrication of high-aspect ratio microneedle molds using low-cost 3D printing. Microsystems Nanoeng 2019 51. 2019;5: 1–14. doi:10.1038/s41378-019-0088-8

4. Haq MI, Smith E, John DN, Kalavala M, Edwards C, Anstey A, et al. Clinical administration of microneedles: skin puncture, pain and sensation. Biomed Microdevices. 2009;11: 35–47. doi:10.1007/s10544-008-9208-1

5. Ahmed Saeed AL-Japairai K, Mahmood S, Hamed Almurisi S, Reddy Venugopal J, Rebhi Hilles A, Azmana M, et al. Current trends in polymer microneedle for transdermal drug delivery. Int J Pharm. 2020;587: 119673. doi:10.1016/J.IJPHARM.2020.119673

6. Larrañeta E, McCrudden M, Courtenay A, Donnelly R. Microneedles: A New Frontier in Nanomedicine Delivery. Pharm Res. 2016;33: 1–19. doi:10.1007/s11095-016-1885-5

7. Yang J, Liu X, Fu Y, Song Y. Recent advances of microneedles for biomedical applications: drug delivery and beyond. Acta Pharm Sin B. 2019;9: 469–483. doi:10.1016/J.APSB.2019.03.007

8. Ye Y, Yu J, Wen D, Kahkoska AR, Gu Z. Polymeric microneedles for transdermal protein delivery. Adv Drug Deliv Rev. 2018;127: 106–118. doi:https://doi.org/10.1016/j.addr.2018.01.015

9. Turner JG, White LR, Estrela P, Leese HS. Hydrogel-Forming Microneedles: Current Advancements and Future Trends. Macromol Biosci. 2021;21: 2000307. doi:https://doi.org/10.1002/mabi.202000307

10. Dardano P, Caliò A, Di Palma V, Bevilacqua MF, Di Matteo A, De Stefano L. A

413 Photolithographic Approach to Polymeric Microneedles Array Fabrication. Mater
414 (Basel, Switzerland). 2015;8: 8661–8673. doi:10.3390/ma8125484

415 11. Wang J, Gong Y, Abba G, Chen K, Shi J, Cai G. Surface Generation Analysis in Micro
416 End-Milling Considering the Influences of Grain. Microsyst Technol. 2008;14: 937–942.
417 doi:10.1007/s00542-007-0478-y

418 12. Lee K, Jung H. Drawing lithography for microneedles: a review of fundamentals and
419 biomedical applications. Biomaterials. 2012;33: 7309–7326.
420 doi:10.1016/j.biomaterials.2012.06.065

421 13. Donnelly RF, Garland MJ, Morrow DIJ, Migalska K, Singh TRR, Majithiya R, et al.
422 Optical coherence tomography is a valuable tool in the study of the effects of
423 microneedle geometry on skin penetration characteristics and in-skin dissolution. J
424 Control release Off J Control Release Soc. 2010;147: 333–341.
425 doi:10.1016/j.jconrel.2010.08.008

426 14. Donnelly RF, Majithiya R, Singh TRR, Morrow DIJ, Garland MJ, Demir YK, et al.
427 Design, optimization and characterisation of polymeric microneedle arrays prepared by
428 a novel laser-based micromoulding technique. Pharm Res. 2011;28: 41–57.
429 doi:10.1007/s11095-010-0169-8

430 15. Wilke N, Mulcahy A, Ye S-R, Morrissey A. Process optimization and characterization
431 of silicon microneedles fabricated by wet etch technology. Microelectronics J. 2005;36:
432 650–656. doi:https://doi.org/10.1016/j.mejo.2005.04.044

433 16. Johnson AR, Procopio AT. Low cost additive manufacturing of microneedle masters.
434 3D Print Med. 2019;5. doi:10.1186/s41205-019-0039-x

435 17. Dabbagh SR, Sarabi MR, Rahbarghazi R, Sokullu E, Yetisen AK, Tasoglu S. 3D-printed

436 microneedles in biomedical applications. iScience. 2021;24: 102012.
437 doi:10.1016/J.ISCI.2020.102012

438 18. Kowsari K, Zhang B, Panjwani S, Chen Z, Hingorani H, Akbari S, et al. Photopolymer
439 formulation to minimize feature size, surface roughness, and stair-stepping in digital
440 light processing-based three-dimensional printing. Addit Manuf. 2018;24: 627–638.
441 doi:10.1016/j.addma.2018.10.037

442 19. Sun A, He X, Ji X, Hu D, Pan M, Zhang L, et al. Current research progress of
443 photopolymerized hydrogels in tissue engineering. Chinese Chem Lett. 2021;32: 2117–
444 2126. doi:10.1016/j.cclet.2021.01.048

445 20. Santra L, Kundu A, Rajaraman S. A Flexible, Digital Light Processing (DLP) 3D Printed
446 and Coated Microneedle Array (CμNA) for Precision Delivery of Novel
447 Nanotherapeutics to Plant Tissue. Proceedings of the IEEE International Conference on
448 Micro Electro Mechanical Systems (MEMS). 2021. pp. 630–633.
449 doi:10.1109/MEMS51782.2021.9375404

450 21. Sirbubalo M, Tucak A, Muhamedagic K, Hindija L, Rahić O, Hadžiabdić J, et al. 3D
451 Printing—a "Touch-Button" Approach To Manufacture Microneedles for Transdermal
452 Drug Delivery. Pharmaceutics. 2021;13: 924. doi:10.3390/pharmaceutics13070924

453 22. Yang Q, Zhong W, Xu L, Li H, Yan Q, She Y, et al. Recent progress of 3D-printed
454 microneedles for transdermal drug delivery. Int J Pharm. 2021;593: 120106.
455 doi:10.1016/J.IJPHARM.2020.120106

456 23. Shin D, Hyun J. Silk fibroin microneedles fabricated by digital light processing 3D
457 printing. J Ind Eng Chem. 2021;95: 126–133. doi:10.1016/j.jiec.2020.12.011

458 24. Erkus H, Bedir T, Kaya E, Tinaz GB, Gunduz O, Chifiriuc M-C, et al. Innovative

459 transdermal drug delivery system based on amoxicillin-loaded gelatin methacryloyl
460 microneedles obtained by 3D printing. Materialia. 2023;27: 101700.
461 doi:https://doi.org/10.1016/j.mtla.2023.101700

462 25. Fabrication of Microneedle Molds and Polymer Based Biodegradable Microneedle
463 Patches: A Novel Method.

464 26. Meng F, Hasan A, Mahdi Nejadi Babadaei M, Hashemi Kani P, Jouya Talaei A, Sharifi
465 M, et al. Polymeric-based microneedle arrays as potential platforms in the development
466 of drugs delivery systems. J Adv Res. 2020;26: 137–147. doi:10.1016/j.jare.2020.07.017

467 27. Doppalapudi S, Jain A, Khan W, Domb AJ. Biodegradable polymers-an overview.
468 Polym Adv Technol. 2014;25: 427–435. doi:10.1002/pat.3305

469 28. Azizi Machekposhti S, Nguyen AK, Vanderwal L, Stafslien S, Narayan RJ.
470 Micromolding of Amphotericin-B-Loaded Methoxyethylene–Maleic Anhydride
471 Copolymer Microneedles. Pharmaceutics. 2022. doi:10.3390/pharmaceutics14081551

472 29. Liu T, Luo G, Xing M. Biomedical Applications of Polymeric Microneedles for
473 Transdermal Therapeutic Delivery and Diagnosis: Current Status and Future
474 Perspectives. Adv Ther. 2020;3: 1900140. doi:10.1002/ADTP.201900140

475 30. Swain S, Pratap Singh A, Yadav RK. A review on polymer hydrogel and polymer
476 microneedle based transdermal drug delivery system. Mater Today Proc. 2021.
477 doi:10.1016/J.MATPR.2021.10.320

478 31. Zhao X, Lang Q, Yildirimer L, Lin ZY, Cui W, Annabi N, et al. Photocrosslinkable
479 Gelatin Hydrogel for Epidermal Tissue Engineering. Adv Healthc Mater. 2016;5: 108–
480 118. doi:10.1002/adhm.201500005

481 32. Luo Z, Sun W, Fang J, Lee K, Li S, Gu Z, et al. Biodegradable Gelatin Methacryloyl

Microneedles for Transdermal Drug Delivery. Adv Healthc Mater. 2019;8: e1801054. doi:10.1002/adhm.201801054

33. Luo Z, Sun W, Fang J, Lee K, Li S, Gu Z, et al. Biodegradable Gelatin Methacryloyl Microneedles for Transdermal Drug Delivery. 2018;1801054: 1–9. doi:10.1002/adhm.201801054

34. Pepelanova I, Kruppa K, Scheper T, Lavrentieva A. Gelatin-methacryloyl (GelMA) hydrogels with defined degree of functionalization as a versatile toolkit for 3D cell culture and extrusion bioprinting. Bioengineering. 2018;5. doi:10.3390/BIOENGINEERING5030055

35. Sun M, Sun X, Wang Z, Guo S, Yu G, Yang H. Synthesis and properties of gelatin methacryloyl (GelMA) hydrogels and their recent applications in load-bearing tissue. Polymers (Basel). 2018;10. doi:10.3390/POLYM10111290

36. Zhang J, Xiao P. 3D printing of photopolymers. Polym Chem. 2018;9: 1530–1540. doi:10.1039/c8py00157j

37. Zhou J, Allonas X, Ibrahim A, Liu X. Progress in the development of polymeric and multifunctional photoinitiators. Prog Polym Sci. 2019;99: 101165. doi:https://doi.org/10.1016/j.progpolymsci.2019.101165

38. Mau R, Nazir J, Seitz H. Dimensional accuracy of 3D printing of PEGDA parts using Digital Light Processing technology. Trans Addit Manuf Meets Med. 2019;1: 2–3. doi:10.18416/AMMM.2019.1909S03P11

39. Farasatkia A, Kharaziha M, Ashrafizadeh F, Salehi S. Transparent silk/gelatin methacrylate (GelMA) fibrillar film for corneal regeneration. Mater Sci Eng C. 2021;120: 111744. doi:10.1016/j.msec.2020.111744

505 40. Raveendran N, Meinert C, Ipe D, Ivanovski S. Optimization of 3D bioprinting of
506 periodontal ligament cells. Dent Mater. 2019;35. doi:10.1016/j.dental.2019.08.114

507 41. Zu G, Meijer M, Mergel O, Zhang H, Rijn P. 3D-Printable Hierarchical Nanogel-GelMA
508 Composite Hydrogel System. Polymers (Basel). 2021;13: 2508.
509 doi:10.3390/polym13152508

510 42. Xiang Y, Wang W, Gao Y, Zhang J, Zhang J, Bai Z, et al. Production and
511 Characterization of an Integrated Multi-Layer 3D Printed PLGA/GelMA Scaffold
512 Aimed for Bile Duct Restoration and Detection. Front Bioeng Biotechnol. 2020;8: 1–14.
513 doi:10.3389/fbioe.2020.00971

514 43. Sreekumaran S, Radhakrishnan A, Rauf AA, Kurup GM. Nanohydroxyapatite
515 incorporated photocrosslinked gelatin methacryloyl/poly(ethylene glycol)diacrylate
516 hydrogel for bone tissue engineering. Prog Biomater. 2021;10: 43–51.
517 doi:10.1007/s40204-021-00150-x

518 44. Rahali K, Ben Messaoud G, Kahn CJF, Sanchez-Gonzalez L, Kaci M, Cleymand F, et
519 al. Synthesis and Characterization of Nanofunctionalized Gelatin Methacrylate
520 Hydrogels. Int J Mol Sci. 2017;18: 2675. doi:10.3390/ijms18122675

521 45. Luo C, Xie R, Zhang J, Liu Y, Li Z, Zhang Y, et al. Low-Temperature Three-
522 Dimensional Printing of Tissue Cartilage Engineered with Gelatin Methacrylamide.
523 Tissue Eng - Part C Methods. 2020;26: 306–316. doi:10.1089/ten.tec.2020.0053

524 46. Yao W, Li D, Zhao Y, Zhan Z, Jin G, Liang H, et al. 3D Printed multi-functional
525 hydrogel microneedles based on high-precision digital light processing. Micromachines.
526 2020;11: 17. doi:10.3390/mi11010017

527 47. Gao Y, Hou M, Yang R, Zhang L, Xu Z, Kang Y, et al. PEGDA/PVP Microneedles with

528 Tailorable Matrix Constitutions for Controllable Transdermal Drug Delivery. Macromol
529 Mater Eng. 2018;303. doi:10.1002/mame.201800233

530 48. Luo Z, Sun W, Fang J, Lee KJ, Li S, Gu Z, et al. Biodegradable Gelatin Methacryloyl
531 Microneedles for Transdermal Drug Delivery. Adv Healthc Mater. 2019;8: 1–9.
532 doi:10.1002/adhm.201801054

533 49. Yan G, Warner KS, Zhang J, Sharma S, Gale BK. Evaluation needle length and density
534 of microneedle arrays in the pretreatment of skin for transdermal drug delivery. Int J
535 Pharm. 2010;391: 7–12. doi:10.1016/j.ijpharm.2010.02.007

536 50. Krieger KJ, Bertollo N, Dangol M, Sheridan JT, Lowery MM, O'Cearbhaill ED. Simple
537 and customizable method for fabrication of high-aspect ratio microneedle molds using
538 low-cost 3D printing. Microsystems Nanoeng. 2019;5. doi:10.1038/s41378-019-0088-8

539 51. Johnson AR, Caudill CL, Tumbleston JR, Bloomquist CJ, Moga KA, Ermoshkin A, et
540 al. Single-step fabrication of computationally designed microneedles by continuous
541 liquid interface production. PLoS One. 2016;11: 1–17.
542 doi:10.1371/journal.pone.0162518

543 52. Lee JW, Park JH, Prausnitz MR. Dissolving microneedles for transdermal drug delivery.
544 Biomaterials. 2008;29: 2113–2124. doi:10.1016/j.biomaterials.2007.12.048

545 53. Sheth S, Jain E, Karadaghy A, Syed S, Stevenson H, Zustiak SP. UV Dose Governs UV-
546 Polymerized Polyacrylamide Hydrogel Modulus. Int J Polym Sci. 2017;2017: 1–9.

547 54. Chansoria P, Asif S, Polkoff K, Chung J, Piedrahita JA, Shirwaiker RA. Characterizing
548 the Effects of Synergistic Thermal and Photo-Cross-Linking during Biofabrication on
549 the Structural and Functional Properties of Gelatin Methacryloyl (GelMA) Hydrogels.
550 ACS Biomater Sci Eng. 2021;7: 5175–5188. doi:10.1021/acsbiomaterials.1c00635

551 55. Li W, Terry RN, Tang J, Feng MR, Schwendeman SP, Prausnitz MR. Rapidly separable
552 microneedle patch for the sustained release of a contraceptive. Nat Biomed Eng. 2019;3:
553 220–229. doi:10.1038/s41551-018-0337-4

554 56. Makvandi P, Kirkby M, Hutton ARJ, Shabani M, Yiu CKY, Baghbantaraghdari Z, et al.
555 Engineering Microneedle Patches for Improved Penetration: Analysis, Skin Models and
556 Factors Affecting Needle Insertion. Nano-Micro Lett. 2021;13: 93. doi:10.1007/s40820-
557 021-00611-9

558 57. Economidou SN, Pissinato Pere CP, Okereke M, Douroumis D. Optimisation of Design
559 and Manufacturing Parameters of 3D Printed Solid Microneedles for Improved Strength,
560 Sharpness, and Drug Delivery. Micromachines. 2021;12. doi:10.3390/mi12020117

561 58. Zhou X, Luo Z, Baidya A, Kim H, Wang C, Jiang X, et al. Biodegradable β-Cyclodextrin
562 Conjugated Gelatin Methacryloyl Microneedle for Delivery of Water-Insoluble Drug.
563 Adv Healthc Mater. 2020;9: 2000527. doi:https://doi.org/10.1002/adhm.202000527

564 59. Zhao ZQ, Zhang BL, Chu HQ, Liang L, Chen BZ, Zheng H, et al. A high-dosage
565 microneedle for programmable lidocaine delivery and enhanced local long-lasting
566 analgesia. Mater Sci Eng C. 2021; 112620.
567 doi:https://doi.org/10.1016/j.msec.2021.112620

568 60. Xenikakis I, Tzimtzimis M, Tsongas K, Andreadis D, Demiri E, Tzetzis D, et al.
569 Fabrication and finite element analysis of stereolithographic 3D printed microneedles for
570 transdermal delivery of model dyes across human skin in vitro. Eur J Pharm Sci.
571 2019;137: 104976. doi:https://doi.org/10.1016/j.ejps.2019.104976

572 61. Gittard SD, Chen B, Xu H, Ovsianikov A, Chichkov BN, Monteiro-Riviere NA, et al.
573 The effects of geometry on skin penetration and failure of polymer microneedles. J
574 Adhes Sci Technol. 2013;27: 227–243. doi:10.1080/01694243.2012.705101

575